# Geometric Stiffness in Interlayer Exciton Condensates

Nishchhal Verma,[1,*] Daniele Guerci,[2,*] and Raquel Queiroz[1,2,†]
[1]Department of Physics, Columbia University, New York, New York 10027, USA
[2]Center for Computational Quantum Physics, Flatiron Institute, New York, New York 10010, USA

(Received 11 September 2023; revised 28 March 2024; accepted 6 May 2024; published 4 June 2024)

Recent experiments have confirmed the presence of interlayer excitons in the ground state of transition metal dichalcogenide bilayers. The interlayer excitons are expected to show remarkable transport properties when they undergo Bose condensation. In this Letter, we demonstrate that quantum geometry of Bloch wave functions plays an important role in the phase stiffness of the interlayer exciton condensate. Notably, we identify a geometric contribution that amplifies the stiffness, leading to the formation of a robust condensate with an increased Berezinskii-Kosterlitz-Thouless temperature. Our results have direct implications for the ongoing experimental efforts on interlayer excitons in materials that have nontrivial quantum geometry. We provide estimates for the geometric contribution in transition metal dichalcogenide bilayers through a realistic continuum model with gated Coulomb interaction, and find that the substantially increased stiffness may allow an interlayer exciton condensate to be realized at amenable experimental conditions.

DOI: 10.1103/PhysRevLett.132.236001

*Introduction.*—Advancements in topological quantum matter have drawn attention to the crucial role of Bloch wave functions in diverse condensed matter systems. While the influence of Berry curvature on noninteracting electrons is well understood as an anomalous velocity [1], a closely related quantity, the quantum metric, has recently gained significant attention, particularly in the context of flatband superconductivity and related experiments in moiré heterostructures [2]. Derived from the geometric properties of Bloch wave functions, the quantum metric has profound effects on various facets of superconductivity. Notably, it modifies the mass of Cooper pairs [3–5], phase stiffness [6–12], spectral weight [13–16], and potentially the critical temperature [17,18]. Other than superconductivity, quantum geometry is known to appear in current noise spectrum [19], dielectric response [20], electron-phonon coupling [21], plasmons [22], and nonlinear response [23–27]. In this Letter, we target interlayer exciton condensates (IECs) and reveal a significant geometric contribution to the phase stiffness that results in a more robust condensate characterized by a higher Berezinskii-Kosterlitz-Thouless (BKT) transition temperature.

Excitons, bound states of electrons and holes in semiconductors, are bosons that have long been proposed to form a BEC at low temperatures [28,29]. Unlike conventional BECs, exciton condensates conserve total particle numbers and instead break a $U(1)_e \times U(1)_h$ symmetry that corresponds to separate conservation of electrons and holes [30,31]. This symmetry is experimentally realizable in a bilayer system with a spacer that suppresses single-particle tunneling between the layers. If the electrons reside on the top ($t$) and holes in bottom ($b$) layers, an IEC is formed by the spontaneous breaking of $U(1)_t \times U(1)_b$ symmetry [32–35]. Its superfluid properties have been observed in quantum Hall systems [36,37].

Although an exciton condensate arising intrinsically in a real material has been a challenge, there has been progress in three-dimensional semimetal 1T-$TiSe_2$ [38], monolayer $WTe_2$ [39,40], bilayer $WSe_2$ [41], and transition metal dichalcogenide (TMD) bilayer $WSe_2/MoSe_2$ [42]. In particular, Ref. [43] has established the existence of interlayer excitons in the ground state by capacitance measurements and characterized the exciton Mott transition [44–48] as a function of the density of electron-hole pairs. These interlayer excitons have finite dipole moments and interact via dipole-dipole interaction. Thus, as a virtue of interacting bosons in 2D, it is possible that there is condensation at low enough temperatures [49–53]. Confirming the existence of the condensate requires transport experiments [31,54], which have remained elusive until two recent reports [55,56].

IECs display fascinating transport properties, most notably dissipationless counterflow transport. When equal and opposite fields are applied to the two layers, excitons flow without resistance in the condensate [36]. The longitudinal counterflow conductivity, $\sigma_{\mathrm{CF}}(\omega)$, diverges in the dc limit with $\sigma_{\mathrm{CF}}(\omega) = D_s\delta(\omega) + \cdots$, where the weight of the delta function, $D_s$, represents the phase stiffness that governs the free energy cost of phase fluctuations in the condensate [57]. In this Letter, we demonstrate that $D_s$, in addition to a conventional contribution from band dispersion, has a significant geometric contribution that arises from the wave functions of the noninteracting electron and hole bands.

The critical role of wave functions in exciton condensation is evident from quantum Hall bilayers where excitons exhibit macroscopic coherence and condense [58,59] despite the noninteracting bands having flat dispersion and infinite mass. The nontrivial wave functions of the Landau level endow mobility to excitons even when the constituent electrons and holes are immobile. Similar phenomenology is anticipated in materials without a magnetic field, such as $WSe_2/MoSe_2$, as a virtue of their nontrivial wave functions [60–62]. However, there are key distinctions due to finite dispersion and asymmetric electron-hole bands, and it remains to be seen if such effects preserve or diminish the geometric contribution. We address these fundamental questions in this Letter.

We begin by deriving the phase stiffness of a general exciton Hamiltonian, separating it into conventional and geometric components. The latter arises primarily from the noninteracting electron and hole wave functions. To demonstrate this effect, we consider a realistic continuum model endowed with screened Coulomb interactions applicable to bilayer TMD devices and provide estimates for the geometric contribution to stiffness in $MoTe_2$ homobilayers [63], as well as $WSe_2/MoSe_2$ heterobilayers [43]. Finally, we propose experimental setups that can serve as validation platforms for our theory.

*Phase stiffness.*—Thermodynamic stability of a condensate depends on the free energy cost associated with spatial fluctuations in the phase, $\theta \to \theta(\mathbf{r})$, which is quantified as $\mathcal{F} = (1/2)D_s \int d\mathbf{r}|\nabla\theta(\mathbf{r})|^2$, where $D_s$ represents the phase stiffness. For IECs, the phase stiffness is calculated as a linear response coefficient when equal and opposite vector potentials are applied to the two layers [37]. The antisymmetric vector potential couples symmetrically to the exciton, since electron and holes have opposite charges, inducing infinitesimal phase fluctuations in the condensate.

A general model Hamiltonian for the IEC is given by $\mathcal{H}_{\text{ex}} = \mathcal{H}_0 + \mathcal{H}_{\text{int}}$, where $\mathcal{H}_0 = \mathcal{H}_t + \mathcal{H}_b$ describes the noninteracting properties with Bloch Hamiltonians $\{\mathcal{H}_\nu\}$ for the two layers $\nu = \{t, b\}$, and $\mathcal{H}_{\text{int}}$ is a density-density interaction that gives rise to excitons. We write $\mathcal{H}_0 = \sum_{\mathbf{k}} \Psi^\dagger_{\mathbf{k}} H_0(\mathbf{k}) \Psi^\dagger_{\mathbf{k}}$, where $H_0(\mathbf{k}) = [H_t(\mathbf{k}) \oplus H_b(\mathbf{k})] + V_b\tau_z$ and $\Psi_{\mathbf{k}}$ is a spinor that has internal labels $(\alpha, \beta)$ that are omitted for brevity along with layer label $\nu$: $\Psi_{\mathbf{k}} = (c_{\mathbf{k},\alpha,t}, \ldots, c_{\mathbf{k},\beta,b}, \cdots)^T$, and $\mathbf{k} \in \text{BZ}$. The last term describes a bias voltage $V_b$ that tunes the gap between the conduction and valence bands (see Fig. 1) with $\tau_z$ being the Pauli matrix in the layer subspace. With vanishing single-particle tunneling between the layers, the noninteracting model has a $U(1)_t \times U(1)_b$ symmetry that is spontaneously broken by the IEC.

Density-density interactions remain unaffected by the external vector potential. Consequently, when equal and opposite $\mathbf{A} = A\hat{x}$ are applied to the two layers, the current operators depend solely on the Bloch Hamiltonian as $H_0(\mathbf{k}, A) = H_t(\mathbf{k} - eA/\hbar) \oplus H_b(\mathbf{k} + eA/\hbar)$. We assume

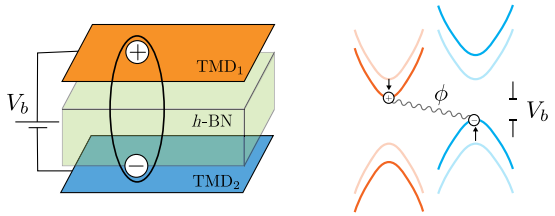


FIG. 1. Device setup with the two layers, orange and blue, with electrons in one and holes in the other. The hexagonal boron nitride ($h$-BN) spacer (green) suppresses single-particle tunneling between the layers. Bias voltage, $V_b$, tunes the gap between lowest unoccupied band and highest occupied band. It is important that these are direct excitons. The bands are shifted horizontally to highlight the layers.

spatially isotropic systems to suppress the tensor nature of currents and stiffness and leave the extension to anisotropic systems to Sec. A6 in Supplemental Material [64]. The current operator can be expressed as $j = -\delta\mathcal{H}_0/\delta A = j_P + Aj_D$, where $j_P = (e/\hbar)\sum_{\mathbf{k}} \Psi^\dagger_{\mathbf{k}}[\tau^z \partial_k \mathcal{H}_0(\mathbf{k})]\Psi_{\mathbf{k}}$ and $j_D = -(e/\hbar)^2 \sum_{\mathbf{k}} \Psi^\dagger_{\mathbf{k}} \partial^2_k \mathcal{H}_0(\mathbf{k}) \Psi_{\mathbf{k}}$ are the paramagnetic and diamagnetic currents, respectively. The stiffness is determined by the Kubo formula, given by $D_s = -[\langle j_D\rangle - \chi_{j_P j_P}(\mathbf{q}_\perp \to 0, \omega = 0)]/4$, where $\chi_{j_P j_P}$ is the longitudinal current-current correlator [57,71,72]. Calculating the stiffness requires a complete enumeration of the eigenstates of the full interacting Hamiltonian $\mathcal{H}_{\text{ex}}$. To make progress beyond the formal definition, we focus on mean-field theories where the interaction term breaks down into fermionic bilinears. We can then utilize the eigenspectrum $E_{m,\mathbf{k}}$ and eigenstates $|u_{m,\mathbf{k}}\rangle$ of the mean-field Hamiltonian to express the stiffness as

$$D_s = \frac{\hbar^2}{4e^2 A}\left[\sum_{\mathbf{k},m} f_{m,\mathbf{k}} \langle u_{m,\mathbf{k}}|\partial^2_k H_0(\mathbf{k})|u_{m,\mathbf{k}}\rangle - \sum_{\mathbf{k},m,n} \frac{f_{m,\mathbf{k}} - f_{n,\mathbf{k}}}{E_{n,\mathbf{k}} - E_{m,\mathbf{k}}} |\langle u_{m,\mathbf{k}}|\tau^z \partial_k H_0(\mathbf{k})|u_{n,\mathbf{k}}\rangle|^2\right], \quad (1)$$

where $f_{m,\mathbf{k}} \equiv f[E_{m,\mathbf{k}}]$ is the Fermi occupation factor and $A$ is the volume normalization factor, which is the area of the sample in 2D. The stiffness measures coherence between transport in the two layers. In the absence of interlayer tunneling, the only way to get finite stiffness is for the interaction to admit an off-diagonal exciton term $\Psi^\dagger_{\mathbf{k}}[\tau^i \hat{\phi}(\mathbf{k})]\Psi_{\mathbf{k}}$ with $i = x, y$ within mean field. The matrix function $\hat{\phi}(\mathbf{k})$ is a mean-field ansatz that needs to be evaluated self-consistently.

Although the dependence of the phase stiffness on wave functions is evident in Eq. (1) from the matrix structure of the current operators, the geometric and energetic terms are intertwined with no clear route to separation. To tackle this challenge, we introduce a projected low-energy model [9], which is applicable when excitons predominantly arise

from the lowest lying electron band ($e$) and the highest hole band ($h$),

$$\mathcal{H}_{\mathrm{ex}} = \sum_{\mathbf{k}} \psi_{\mathbf{k}}^{\dagger} \begin{pmatrix} \epsilon_e(\mathbf{k}) - \Sigma_e(\mathbf{k}) & \varphi(\mathbf{k}) \\ \varphi(\mathbf{k})^* & \epsilon_h(\mathbf{k}) + \Sigma_h(\mathbf{k}) \end{pmatrix} \psi_{\mathbf{k}}, \tag{2}$$

where $\epsilon_{e/h}$ are the bare electron and hole dispersions, $\psi_{\mathbf{k}} = (c_{\mathbf{k},e}, c_{\mathbf{k},h})^T$ is the low-energy basis state, $\Sigma_{e/h}(\mathbf{k})$ are the self-energies (including $V_b$), and $\varphi(\mathbf{k})$ is a shorthand for

$$\varphi(\mathbf{k}) = \sum_{\alpha \in t, \beta \in b} [U_t(\mathbf{k})]^*_{e,\alpha} \phi_{\alpha\beta}(\mathbf{k}) [U_b(\mathbf{k})]_{\beta,h}. \tag{3}$$

A crucial aspect to highlight is that $U_t(\mathbf{k})$ and $U_b(\mathbf{k})$ are independent unitary matrices that diagonalize $H_t(\mathbf{k})$ and $H_b(\mathbf{k})$, respectively. The subscripts $e$ and $h$ indicate the electron and hole bands involved in the exciton pairing. It is important to note that, unlike in BCS theory where the redundancy in Nambu basis introduces a particle-hole symmetry in the Bogoliubov–de Gennes Hamiltonian, $U_t(\mathbf{k})$ and $U_b(\mathbf{k})$ do not have such constraints. Hence our framework is a generalization of phase stiffness that is designed for $WSe_2/MoSe_2$ bilayers where the electron and hole bands originate from distinct materials.

We next assume $\epsilon_e(\mathbf{k}) = -\epsilon_h(\mathbf{k}) = \epsilon(\mathbf{k})$, while allowing $U_t(\mathbf{k})$ to differ from $U_b(\mathbf{k})$. This assumption is justified as the effect of asymmetric dispersion on exciton is a well-understood textbook problem [73] that only complicates our analysis without offering additional insight [64]. On the other hand, the presence of $U_t(\mathbf{k})$ and $U_b(\mathbf{k})$ has a nontrivial consequence for $\varphi(\mathbf{k})$ in the presence of vector potential

$$\varphi(\mathbf{k}, A) \approx \varphi(\mathbf{k}) - \frac{eA}{\hbar} \mathcal{P}(\mathbf{k}) - \frac{e^2 A^2}{2\hbar^2} \mathcal{D}(\mathbf{k}), \tag{4}$$

where $\mathcal{P}(\mathbf{k})$ and $\mathcal{D}(\mathbf{k})$ are the paramagnetic and diamagnetic terms that involve derivatives of $U_\nu(\mathbf{k})$ (Sec. A2 in Supplemental Material [64] has the full expression). These terms are in addition to the energetic terms arising from $\partial_k \epsilon(\mathbf{k})$ and $\partial_k^2 \epsilon(\mathbf{k})$ in the current operator and are key to our analysis. After performing a lengthy but straightforward calculation [64], we find two main contributions to the stiffness $D_s = D_s^c + D_s^g$ with

$$D_s^c = \frac{1}{2A} \sum_{\mathbf{k}} \partial_{k_i}^2 \epsilon(\mathbf{k}) v_{\mathbf{k}}^2 \tag{5}$$

$$D_s^g = \frac{1}{4A} \sum_{\mathbf{k}} \frac{\mathcal{G}(\mathbf{k})}{E(\mathbf{k})} + \frac{1}{4A} \sum_{\mathbf{k}} \frac{\mathrm{Re}[\mathcal{P}(\mathbf{k}) \varphi(\mathbf{k})^*]^2}{E(\mathbf{k})^3}, \tag{6}$$

where $v_{\mathbf{k}}^2 = [1 - \xi(\mathbf{k})/E(\mathbf{k})]/2$ is the momentum occupation factor with $\xi(\mathbf{k}) = \epsilon(\mathbf{k}) - \Sigma(\mathbf{k})$, and $E(\mathbf{k}) = \sqrt{\xi(\mathbf{k})^2 + |\varphi(\mathbf{k})|^2}$ is the mean-field quasiparticle dispersion. The second part of the equation includes the geometric quantity $\mathcal{G}(\mathbf{k}) = \mathrm{Re}[\mathcal{D}(\mathbf{k}) \varphi(\mathbf{k})^*] - |\mathcal{P}(\mathbf{k})|^2$. We note that all terms in Eq. (6) are individually gauge invariant and constitute the main result of our Letter [64].

A few comments are in order. The geometric contribution in Eq. (6) arises explicitly from the Taylor expansion of the off-diagonal term $\varphi(\mathbf{k}, A)$. If the wave functions were trivial, say independent of $\mathbf{k}$, this contribution would vanish since $\mathcal{P}(\mathbf{k}) = \mathcal{D}(\mathbf{k}) = 0$.

As one might expect, there are some connections with superconductivity as well. If the bands were particle-hole symmetric, Eq. (2) would reduce to a Bogoliubov–de Gennes matrix and the function $\mathcal{G}(\mathbf{k})$ will become precisely the quantum metric, $g(\mathbf{k})$. This is not surprising since superfluid stiffness is known to be enhanced by quantum metric in superconductors within mean field [2]. Since the particle-hole symmetry is not enforced in an exciton mean-field theory, our results present a generalization of quantum geometric phase stiffness beyond pairing between particle-hole symmetric states.

We further note that orbital embedding modifies our calculation in a similar fashion as in superconductivity [11]. It enforces the minimal condition where the solution to gap equation is kept real in the presence of external vector potential [74]. Our result demonstrate a generalization of excitonic phase stiffness beyond particle-hole symmetry discussed in the context of quantum Hall bilayers [58].

*Hubbard model with tunable quantum metric.*—To illustrate the phenomenology with a simple model, we consider an interlayer on-site orbital-diagonal Hubbard interaction $\mathcal{H}_{\mathrm{int}} = V \sum_{\mathbf{i},\alpha} \hat{n}_{\mathbf{i},\alpha,t} \hat{n}_{\mathbf{i},\alpha,b}$. The labels $\mathbf{i}$, $\alpha$ pertaining to unit cell index and orbitals, are not crucial for our discussion as long as the interaction is interlayer in character [64].

For the Bloch hamiltonian, we consider a tunable quantum metric model that has two orbitals on a square lattice with the Bloch Hamiltonian

$$H(\zeta, \mathbf{k}) = 2t(2 - p_{\mathbf{k}}) + t_F \cos(\zeta p_{\mathbf{k}}) \sigma^x + t_F \sin(\zeta p_{\mathbf{k}}) \sigma^y, \tag{7}$$

where the Pauli matrices $\sigma^i$ act in orbital space, $p_{\mathbf{k}}$ is a periodic function given by $p_{\mathbf{k}} = \cos k_x + \cos k_y$, and the parameter $\zeta$ controls the quantum geometry by introducing long range hoppings [75]. More precisely, $\zeta$ is an overall scaling factor for the quantum geometric tensor $\mathcal{Q}(\mathbf{k}, \zeta)_{\mu\nu} = (\zeta^2/4) \sin k_\mu \sin k_\nu$, which is real because of inversion and time-reversal symmetries. The Berry curvature $F(\mathbf{k}) = -\mathrm{Im}[\mathcal{Q}(\mathbf{k})]_{xy}/2$ vanishes identically while the quantum metric $g_{\mu\nu}(\mathbf{k}) = \mathrm{Re}[\mathcal{Q}_{\mathbf{k}}]_{\mu\nu}$ is finite. Another convenient aspect of this model is that the band dispersions $\epsilon_{\pm,\mathbf{k}} = 2t(2 - p_{\mathbf{k}}) \pm t_F$ are independent of $\zeta$. This permits the use of $\zeta$ to tune quantum geometry without affecting the band dispersion, capturing the discussion around Eq. (6).

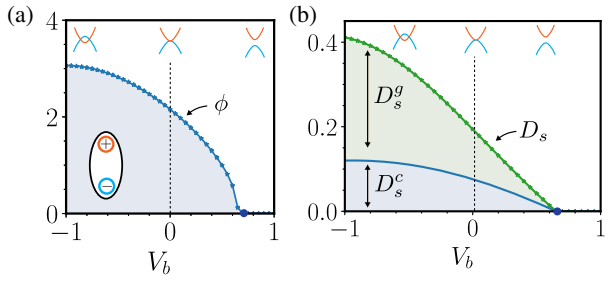


FIG. 2. (a) Mean-field gap solution for the toy model with tunable quantum metric at fixed interaction $U = 6t$. (b) Mean-field phase stiffness. All energy scales, $\phi$, $D_s$, $V_b$, are plotted in units of single-particle hopping $t$ [see Eq. (7)]. Subscripts $c$ and $g$ denote conventional and geometric contributions respectively.

Symmetric bilayers, where both layers are described by the same parameter $\zeta$, give rise to excitons [see Fig. 2(a)], where the stiffness has a significant enhancement coming from the geometric term $D_s^g$. The extra contribution is indeed proportional to the trace of the quantum metric in this particular case, as Eq. (6) simplifies to $D_s^g = (\phi^2/4A)\sum_{\mathbf{k}} g(\mathbf{k})/E(\mathbf{k})$ [76]. While the geometric contribution dominates at higher bias voltage $|V_b|$, it is important to note that a high $|V_b|$ results in higher densities of electron-hole pairs and may ultimately drive the system to the exciton Mott transition [45–48]. The case of asymmetric wave functions follows along similar lines and is outlined in Fig. S3 [64].

*Continuum model for TMDs.*—With the formalism in place, we now aim to quantify the role of quantum geometric effects in TMD exciton bilayers. TMDs are semiconductors with valley optical selection rules [77] and hence their minimal model is that of a gapped Dirac cone. We consider the continuum Hamiltonian introduced in Ref. [78] with spin-valley locking. The continuum $k.p$ Hamiltonian for a given spin and valley, to first order in $k$, reads

$$H_\nu(\mathbf{k}) = \Delta_\nu \sigma_z + v_\nu k \cdot \sigma, \tag{8}$$

where $\sigma^i$ is the Pauli matrix in the internal sublattice degrees of freedom for the conduction and valence bands, and dispersion $\epsilon_{\mathbf{k}\nu\pm} = \pm\sqrt{\Delta_\nu^2 + v_\nu^2|\mathbf{k}|^2}$. The two-band aspect of the model is justified for the valence band where the Ising spin-orbit coupling gap is of the order of 180 meV in $MoX_2$ and 440 meV in $WX_2$ [79]. We also neglect the quadratic trigonal warping term and the quadratic particle-hole mass imbalance since it does not play an important role in our phenomenological discussion.

The geometric properties of the model are encoded in the form factors $F^\nu_{\mathbf{k},\mathbf{q}} = U^\dagger_\nu(\mathbf{k})U_\nu(\mathbf{k}+\mathbf{q})$, which have nontrivial momentum dependence. In order to isolate the geometric contribution, we will compare our results with the gapped Dirac cone in Eq. (8) to that of a parabolic band $H_\nu(\mathbf{k}) = \pm\epsilon_{\mathbf{k}\nu}\sigma_z$ with energies $\epsilon_{\mathbf{k}\nu} \approx \Delta_\nu + k^2/2m_\nu$ with $m_\nu = v_\nu^2/m_\nu$ and trivial form factor $F^\nu_{\mathbf{k},\mathbf{q}} = \delta_{\mathbf{k},\mathbf{q}}$.

We overlay this model with a gated Coulomb interaction,

$$\mathcal{H}_{\text{int}} = \frac{1}{2A}\sum_{\mathbf{q}}^{\Lambda}\sum_{\nu,\nu'=t,b} V^{\nu\nu'}_{\mathbf{q}}\hat{n}_{\mathbf{q},\nu}\hat{n}_{-\mathbf{q},\nu'}, \tag{9}$$

where $\hat{n}_{\mathbf{q},\nu}$ is the layer resolved density operator $\hat{n}_{\mathbf{q},\nu} = \sum_{\mathbf{k}}^{\Lambda}\sum_{a=K,K'}\psi^\dagger_{\mathbf{k},a\nu}\psi_{\mathbf{k}+\mathbf{q},a\nu}$ and

$$V^{tt}_{\mathbf{q}} = V^{bb}_{\mathbf{q}} = \frac{e^2}{\epsilon\epsilon_0}\frac{\tanh\frac{q\xi}{2}}{2q}, \quad V^{tb}_{\mathbf{q}} = V^{bt}_{\mathbf{q}} = e^{-dq}V^{tt}_{\mathbf{q}}. \tag{10}$$

Here, $d$ is the interlayer distance, $\Lambda$ is the UV cutoff, and $\xi$ is the screening length of the bilayer, which is defined as the distance between the bilayer and the metallic gates. As representative values [41,43], we set $\xi = 12$ nm, $\epsilon \approx 6$, and $d \approx 1$ nm. We focus on the regime of low density of electron-hole pairs $n_{\text{e-h}} \leq 0.075$ to reduce screening effects leading to the exciton Mott transition [44–48]. We now proceed with a Hartree-Fock calculation. We find that while the Hartree term vanishes as a consequence of charge neutrality, the Fock term gives rise to a self-energy correction to the single-particle Hamiltonian. The self-consistent equations for the Fock self-energy are solved employing an iterative scheme [64].

The Coulomb interaction induces intravalley excitons as well as charge transfer between the two layers $\phi_z = \langle\tau^z\sigma^0\rangle = 2n_{\text{e-h}}$. The operators $\tau^\pm\sigma^a$ probe spontaneous interlayer coherence where $\tau^\pm = (\tau^x \pm i\tau^y)/2$ are raising or lowering operators in the layer degree of freedom and $\sigma^a$ are Pauli matrices in the band space. A finite expectation value $\langle\tau^\pm\sigma^a\rangle \neq 0$ corresponds to an interlayer intravalley exciton condensate that breaks the $U(1)_{e/h}$ symmetry. The first panel of Fig. 3 shows the evolution of $\phi = \sqrt{\sum_{a=x,y,z}\langle\tau^x\sigma^a\rangle^2}$ in the gauge where interlayer symmetry is broken along $\tau^x$ as a function of $V_b$ for the homobilayer [Fig. 3(a)] and heterobilayer [Fig. 3(b)] case. We notice that for the continuum theory the energy $V_b$ is given by $V_b = (\Delta_t + \Delta_b - 2E_z)/2$ with $E_z$ electric displacement field applied to the bilayer. Above a critical value of the electrostatic potential $V_b^* \approx 70/75$ meV the system turns into a semiconductor where the energy gap $E_{\text{gap}}$ grows linearly with the applied bias. Finally, the phase stiffness is calculated using Eq. (1) where the expectation value is taken with the Hartree-Fock wave functions. The results are shown in the right panel of Figs. 3(a) and 3(b), blue data for parabolic bands and green for a gapped Dirac cone. We emphasize that the nontrivial structure of the wave functions appears in the geometric contribution of the superfluid stiffness, while it does not change the exciton binding energy (energy gap) and the size of the order parameter.

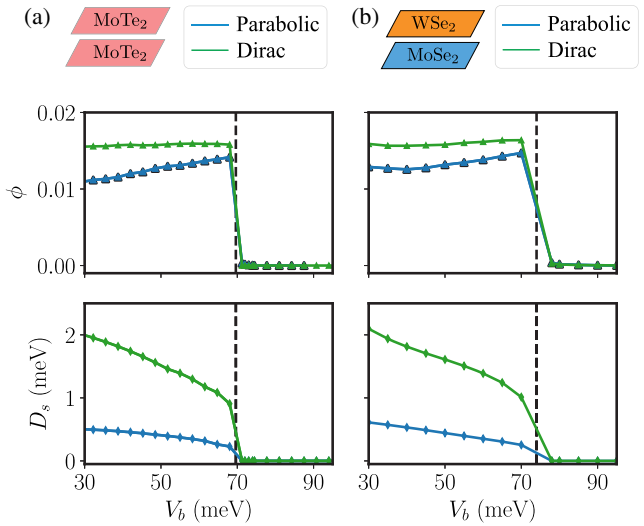


FIG. 3. We show the interlayer exciton coherence $\phi$ and the phase stiffness $D_s$ as a function of $V_b$. Green and Blue data corresponds to a gapped Dirac cone and parabolic bands with mass $m = v^2/\Delta$, respectively. **a**: Homobilayer with velocity $v = 2.16$ eV Å, energy gap $\Delta = 0.9$ eV relevant for $MoTe_2$. **b**: Heterobilayer with velocity $v_t = 2.2$ eV Å and $v_b = 2.6$ eV Å, energy gap $\Delta_t = 1.21$ eV and $\Delta_b = 1.16$ eV representative values for $WSe_2/MoSe_2$. In both cases, we find spontaneous formation of excitons around $V_b^* \approx 70/75$ meV. The calculations were done with gate distance $\xi = 12$ nm and spacing between the two layers $d = 1$ nm.

Remarkably, the geometric component increases $D_s$ and, correspondingly, the BKT transition temperature ($T_{\mathrm{BKT}}$) related to the superfluid stiffness by the Nelson-Kosterlitz relation $k_B T_{\mathrm{BKT}} = \pi/2[\lim_{T\to T_{\mathrm{BKT}}^-} D_s(T)]$ [80]. Approximating $D_s(T)$ with its $T = 0$ value [from last panel in Fig. 3(b), we infer that geometric contribution increases $T_{\mathrm{BKT}}$ roughly from 12 to 36 K at $V_b \approx 40$ meV. This threefold increase should be observable in experiments.

*Conclusion.*—Phase stiffness is significantly modified by the constituent electron and hole wave functions of the exciton. We investigated two limiting scenarios, one with local Hubbard interaction and the other with gated Coulomb interaction projected onto the low-energy bands, and remarkably, we find geometric contributions that play a vital role in either case. Our findings complement existing research on the effects of quantum geometry in exciton spectrum [81–83], exciton wave function [84] and its possible realizations in moiré heterostructures [76,85,86]. Importantly, we find a gauge-invariant quantum geometric quantity $\mathcal{G}(\mathbf{k})$ whose properties require further investigation.

Bilayer TMD devices offer an ideal platform to validate our predictions. However, unlike theoretical models where wave functions can be turned off explicitly, isolating the geometric component from experimental data is a big challenge [87]. One key observation from our numerics is that the exciton binding energy ($\phi$) is mostly unaffected by the wave functions, in stark contrast to superfluid stiffness ($D_s$) (Fig. 3). This feature should lead to a discrepancy between $\phi$ and $D_s$, and more generally, between thermodynamic (capacitance) and transport probes (counterflow). The enhancement in $D_s$ should raise the BKT transition temperature. Quite recently, two experiments [55,56] have claimed perfect drag in $MoSe_2/WSe_2$ bilayers around 20 K. If the perfect drag is a result of exciton condensation, our calculations indicate that the quantum geometry of TMDs is essential in estimating the onset temperature. Another avenue for isolating the geometric contribution can be critical counterflow current experiments using nonlinear transport similar to studies in twisted bilayer graphene superconductor [88].

Research on geometric properties of exciton condensates is supported as part of Programmable Quantum Materials, an Energy Frontier Research Center funded by the U.S. Department of Energy (DOE), Office of Science, Basic Energy Sciences (BES), under Award No. DE-SC0019443. We benefited from the 2023 Quantum Geometry Working Group meeting that took place at the Flatiron Institute. We thank Päivi Törmä and Jonah Herzog-Arbeitman for their comments on orbital embeddings and minimal quantum metric. We acknowledge discussions with Kin Fai Mak, Pavel Volkov, Yongxin Zeng, and Ilia Komissarov. D. G. and R. Q. acknowledge support from the Flatiron Institute, a division of the Simons Foundation.

*These authors contributed equally to this work.
†Corresponding author: raquel.queiroz@columbia.edu

[1] D. Xiao, M.-C. Chang, and Q. Niu, Rev. Mod. Phys. **82**, 1959 (2010).
[2] P. Törmä, S. Peotta, and B. A. Bernevig, Nat. Rev. Phys. **4**, 528 (2022).
[3] P. Törmä, L. Liang, and S. Peotta, Phys. Rev. B **98**, 220511 (R) (2018).
[4] M. Iskin, Phys. Rev. A **97**, 033625 (2018).
[5] M. Iskin, Phys. Rev. A **103**, 053311 (2021).
[6] S. Peotta and P. Törmä, Nat. Commun. **6**, 8944 (2015).
[7] A. Julku, S. Peotta, T. I. Vanhala, D.-H. Kim, and P. Törmä, Phys. Rev. Lett. **117**, 045303 (2016).
[8] L. Liang, T. I. Vanhala, S. Peotta, T. Siro, A. Harju, and P. Törmä, Phys. Rev. B **95**, 024515 (2017).
[9] F. Xie, Z. Song, B. Lian, and B. A. Bernevig, Phys. Rev. Lett. **124**, 167002 (2020).
[10] J. Herzog-Arbeitman, V. Peri, F. Schindler, S. D. Huber, and B. A. Bernevig, Phys. Rev. Lett. **128**, 087002 (2022).
[11] K.-E. Huhtinen, J. Herzog-Arbeitman, A. Chew, B. A. Bernevig, and P. Törmä, Phys. Rev. B **106**, 014518 (2022).
[12] D. Mao and D. Chowdhury, Proc. Natl. Acad. Sci. U.S.A. **120**, e2217816120 (2023).
[13] M. Tovmasyan, S. Peotta, P. Törmä, and S. D. Huber, Phys. Rev. B **94**, 245149 (2016).
[14] N. Verma, T. Hazra, and M. Randeria, Proc. Natl. Acad. Sci. U.S.A. **118**, e2106744118 (2021).
[15] J. Ahn and N. Nagaosa, Phys. Rev. B **104**, L100501 (2021).

[16] D. Mao and D. Chowdhury, Phys. Rev. B **109**, 024507 (2024).
[17] J. S. Hofmann, E. Berg, and D. Chowdhury, Phys. Rev. B **102**, 201112(R) (2020).
[18] V. Peri, Z.-D. Song, B. A. Bernevig, and S. D. Huber, Phys. Rev. Lett. **126**, 027002 (2021).
[19] T. Neupert, C. Chamon, and C. Mudry, Phys. Rev. B **87**, 245103 (2013).
[20] I. Komissarov, T. Holder, and R. Queiroz, arXiv: 2306.08035.
[21] J. Yu, C. J. Ciccarino, R. Bianco, I. Errea, P. Narang, and B. A. Bernevig, arXiv:2305.02340.
[22] A. Arora, M. S. Rudner, and J. C. W. Song, Nano Lett. **22**, 9351 (2022).
[23] M. F. Lapa and T. L. Hughes, Phys. Rev. B **99**, 121111(R) (2019).
[24] Y. Gao and D. Xiao, Phys. Rev. Lett. **122**, 227402 (2019).
[25] V. Kozii, A. Avdoshkin, S. Zhong, and J. E. Moore, Phys. Rev. Lett. **126**, 156602 (2021).
[26] J. Ahn, G.-Y. Guo, N. Nagaosa, and A. Vishwanath, Nat. Phys. **18**, 290 (2022).
[27] S. Chaudhary, C. Lewandowski, and G. Refael, Phys. Rev. Res. **4**, 013164 (2022).
[28] J. M. Blatt, K. W. Böer, and W. Brandt, Phys. Rev. **126**, 1691 (1962).
[29] B. I. Halperin and T. M. Rice, Rev. Mod. Phys. **40**, 755 (1968).
[30] Y. E. Lozovik and V. Yudson, JETP Lett. (USSR) (Engl. Transl.) **22**, 556 (1975).
[31] Y. E. Lozovik and V. Yudson, Zh. Eksp. Teor. Fiz. **71**, 738 (1976).
[32] D. Yoshioka and A. H. MacDonald, J. Phys. Soc. Jpn. **59**, 4211 (1990).
[33] K. Yang, Phys. Rev. Lett. **87**, 056802 (2001).
[34] S. De Palo, F. Rapisarda, and G. Senatore, Phys. Rev. Lett. **88**, 206401 (2002).
[35] Y. N. Joglekar, A. V. Balatsky, and S. Das Sarma, Phys. Rev. B **74**, 233302 (2006).
[36] J. P. Eisenstein and A. H. MacDonald, Nature (London) **432**, 691 (2004).
[37] J. P. Eisenstein, Annu. Rev. Condens. Matter Phys. **5**, 159 (2014).
[38] A. Kogar, M. S. Rak, S. Vig, A. A. Husain, F. Flicker, Y. I. Joe, L. Venema, G. J. MacDougall, T. C. Chiang, E. Fradkin, J. Van Wezel, and P. Abbamonte, Science **358**, 1314 (2017).
[39] Y. Jia *et al.*, Nat. Phys. **18**, 87 (2022).
[40] B. Sun, W. Zhao, T. Palomaki, Z. Fei, E. Runburg, P. Malinowski, X. Huang, J. Cenker, Y.-T. Cui, J.-H. Chu, X. Xu, S. S. Ataei, D. Varsano, M. Palummo, E. Molinari, M. Rontani, and D. H. Cobden, Nat. Phys. **18**, 94 (2022).
[41] Q. Shi, E.-M. Shih, D. Rhodes, B. Kim, K. Barmak, K. Watanabe, T. Taniguchi, Z. Papić, D. A. Abanin, J. Hone, and C. R. Dean, Nat. Nanotechnol. **17**, 577 (2022).
[42] Z. Wang, D. A. Rhodes, K. Watanabe, T. Taniguchi, J. C. Hone, J. Shan, and K. F. Mak, Nature (London) **574**, 76 (2019).
[43] L. Ma, P. X. Nguyen, Z. Wang, Y. Zeng, K. Watanabe, T. Taniguchi, A. H. MacDonald, K. F. Mak, and J. Shan, Nature (London) **598**, 585 (2021).
[44] N. F. Mott, Proc. Phys. Soc. London Sect. A **62**, 416 (1949).
[45] N. F. Mott, Contemp. Phys. **14**, 401 (1973).
[46] W. F. Brinkman and T. M. Rice, Phys. Rev. B **7**, 1508 (1973).
[47] L. M. Smith and J. P. Wolfe, Phys. Rev. Lett. **57**, 2314 (1986).
[48] D. Guerci, M. Capone, and M. Fabrizio, Phys. Rev. Mater. **3**, 054605 (2019).
[49] P. Nozieres and S. Schmitt-Rink, J. Low Temp. Phys. **59**, 195 (1985).
[50] M. M. Fogler, L. V. Butov, and K. S. Novoselov, Nat. Commun. **5**, 4555 (2014).
[51] F.-C. Wu, F. Xue, and A. H. MacDonald, Phys. Rev. B **92**, 165121 (2015).
[52] O. L. Berman and R. Y. Kezerashvili, Phys. Rev. B **93**, 245410 (2016).
[53] B. Debnath, Y. Barlas, D. Wickramaratne, M. R. Neupane, and R. K. Lake, Phys. Rev. B **96**, 174504 (2017).
[54] A. A. High, J. R. Leonard, A. T. Hammack, M. M. Fogler, L. V. Butov, A. V. Kavokin, K. L. Campman, and A. C. Gossard, Nature (London) **483**, 584 (2012).
[55] P. X. Nguyen, L. Ma, R. Chaturvedi, K. Watanabe, T. Taniguchi, J. Shan, and K. F. Mak, arXiv:2309.14940.
[56] R. Qi, A. Y. Joe, Z. Zhang, J. Xie, Q. Feng, Z. Lu, Z. Wang, T. Taniguchi, K. Watanabe, S. Tongay *et al.*, arXiv:2309 .15357.
[57] D. J. Scalapino, S. R. White, and S. Zhang, Phys. Rev. B **47**, 7995 (1993).
[58] H. A. Fertig, Phys. Rev. B **40**, 1087 (1989).
[59] I. B. Spielman, J. P. Eisenstein, L. N. Pfeiffer, and K. W. West, Phys. Rev. Lett. **87**, 036803 (2001).
[60] D. Xiao, W. Yao, and Q. Niu, Phys. Rev. Lett. **99**, 236809 (2007).
[61] T. Cao, G. Wang, W. Han, H. Ye, C. Zhu, J. Shi, Q. Niu, P. Tan, E. Wang, B. Liu, and J. Feng, Nat. Commun. **3**, 887 (2012).
[62] G. Wang, A. Chernikov, M. M. Glazov, T. F. Heinz, X. Marie, T. Amand, and B. Urbaszek, Rev. Mod. Phys. **90**, 021001 (2018).
[63] C. Robert, R. Picard, D. Lagarde, G. Wang, J. P. Echeverry, F. Cadiz, P. Renucci, A. Högele, T. Amand, X. Marie, I. C. Gerber, and B. Urbaszek, Phys. Rev. B **94**, 155425 (2016).
[64] See Supplemental Material at http://link.aps.org/supplemental/10.1103/PhysRevLett.132.236001 for a detailed discussion, which includes Refs. [65–70].
[65] Z. Sun, T. Kaneko, D. Golež, and A. J. Millis, Phys. Rev. Lett. **127**, 127702 (2021).
[66] S. H. Simon and M. S. Rudner, Phys. Rev. B **102**, 165148 (2020).
[67] B. S. Chandrasekhar, Appl. Phys. Lett. **1**, 7 (1962).
[68] A. M. Clogston, Phys. Rev. Lett. **9**, 266 (1962).
[69] Y. Liang, S. Huang, R. Soklaski, and L. Yang, Appl. Phys. Lett. **103**, 042106 (2013).
[70] T. Cheiwchanchamnangij and W. R. L. Lambrecht, Phys. Rev. B **85**, 205302 (2012).
[71] L. Benfatto, A. Toschi, and S. Caprara, Phys. Rev. B **69**, 184510 (2004).
[72] T. Cea, C. Castellani, G. Seibold, and L. Benfatto, Phys. Rev. Lett. **115**, 157002 (2015).
[73] M. A. M. Fox, *Optical Properties of Solids* (Oxford University Press, New York, 2001), Chap. 4.

[74] S. Peotta, New J. Phys. **24**, 113019 (2022).
[75] J. S. Hofmann, E. Berg, and D. Chowdhury, Phys. Rev. Lett. **130**, 226001 (2023).
[76] X. Hu, T. Hyart, D. I. Pikulin, and E. Rossi, Phys. Rev. B **105**, L140506 (2022).
[77] D. Xiao, G.-B. Liu, W. Feng, X. Xu, and W. Yao, Phys. Rev. Lett. **108**, 196802 (2012).
[78] X. Zhu, P. B. Littlewood, M. S. Hybertsen, and T. M. Rice, Phys. Rev. Lett. **74**, 1633 (1995).
[79] A. Kormányos, G. Burkard, M. Gmitra, J. Fabian, V. Zólyomi, N. D. Drummond, and V. Fal'ko, 2D Mater. **2**, 022001 (2015).
[80] D. R. Nelson and J. M. Kosterlitz, Phys. Rev. Lett. **39**, 1201 (1977).
[81] J. Zhou, W.-Y. Shan, W. Yao, and D. Xiao, Phys. Rev. Lett. **115**, 166803 (2015).
[82] A. Srivastava and A. Imamoğlu, Phys. Rev. Lett. **115**, 166802 (2015).
[83] W. Yao and Q. Niu, Phys. Rev. Lett. **101**, 106401 (2008).
[84] G. Sethi, M. Cuma, and F. Liu, Phys. Rev. Lett. **130**, 186401 (2023).
[85] Y. H. Kwan, Y. Hu, S. H. Simon, and S. A. Parameswaran, Phys. Rev. Lett. **126**, 137601 (2021).
[86] X. Hu, E. Rossi, and Y. Barlas, arXiv:2304.04825.
[87] P. Törmä, Phys. Rev. Lett. **131**, 240001 (2023).
[88] H. Tian, X. Gao, Y. Zhang, S. Che, T. Xu, P. Cheung, K. Watanabe, T. Taniguchi, M. Randeria, F. Zhang, C. N. Lau, and M. W. Bockrath, Nature (London) **614**, 440 (2023).